Nanoscale Research Letters

NANO EXPRESS Open Access

A Multi-level Memristor Based on Al-Doped HfO_2 Thin Film

Lei Wu, Hongxia Liu*, Jiabin Li, Shulong Wang and Xing Wang

Abstract

Non-volatile memory (NVM) will play a very important role in the next-generation digital technologies, including the Internet of things. The metal-oxide memristors, especially based on HfO_2, have been favored by lots of researchers because of its simple structure, high integration, fast operation speed, low power consumption, and high compatibility with advanced (complementary metal oxide silicon) CMOS technologies. In this paper, a 20-level stable resistance states Al-doped HfO_2-based memristor is presented. Its cycles endurance, data retention time, and resistance ratio are larger than 10^3, $> 10^4$ s, and > 10, respectively.

Keyword: Memristor, HfO_2, Al doped, Multi-level memory

Background

Although negative resistance phenomenon firstly was discovered by Hickmott in an $Al/Al_2O_3/Au$ structure in 1962 [1], and Chua proposed the concept of memristor in 1971 [2]. It was not until Strukov et al prepared the TiO_2-based memristor in 2008 [3] that people began to pay attention to the study on memristors. At present, researchers have prepared memristors with more than dozens of active resistive materials, including multiple complex oxides [4, 5], metal oxides such as ZnO [6], TiO_x [7], TaO_x [8], and two-dimensional materials [9, 10]. HfO_2 has been used as high-k gate dielectrics in CMOS devices since its high reliability, fast operation speed, and low-power consumption [11, 12]. It is also preferred by researchers as a memristive material [13–15].

Multi-level memristor can be widely used as data storage [16–18], logical calculation [19], electronic synaptic device [20–23], and so on. Wang Y. [16] and Gao B. et al. [24] prepared multi-level memristors by doping HfO_2 with Cu and Gd, respectively, but they can only create 4-level storage state, which is difficult to meet the demands of the applications. Therefore, the study on HfO_2 multi-level memristors is of great significance.

Methods

$Ti/Al:HfO_2/Pt$ device was fabricated as shown in Fig. 1a. The active cell area was defined by the square-shaped Ti top electrode (TE). A 20-nm Ti adhesive layer was deposited by direct current (DC) sputtering on a silicon substrate, then a 100-nm Pt film was deposited as a bottom electrode (BE). The 20-nm Al-doped HfO_2 functional layer was deposited by the atomic layer deposition (ALD) reactor (R-150, Picosun, Espoo, Finland) at 300 °C with $MeCp_2HfMe(OMe)$ (denoted as HfD-04) as Hf precursor, and H_2O as oxygen source [25]. The precursors were carried by high-purity N_2 (> 99.999%) into the reactor chamber. Al-doped films were obtained by depositing one cycle of Al_2O_3 at every 8 cycles of HfO_2 with the trimethylaluminum (TMA) as the Al source and H_2O as oxygen source. The Al atomic concentration of 6.2% is detected by X-ray photoelectron spectroscopy (XPS, Axis Ultra DLD, Kratos Analytical, Manchester, UK) on a Theta 300 XPS system from Thermo Fisher. A 50-nm Ti film as TE and 100 nm Pt as covering layer were deposited by DC sputtering. Devices are obtained by patterning the TE by optical lithography and lift-off process. Figure 1b is the optical micrograph of the devices. We have prepared devices with different areas ranging from 5 μm × 5 μm to 500 μm × 500 μm.

Results and Discussion

Figure 2 shows the XPS of Al-doped and non-doped devices. Comparing to the spectrograms of non-doped

* Correspondence: hxliu@mail.xidian.edu.cn
Key Laboratory for Wide-Band Gap Semiconductor Materials and Devices of Education, School of Microelectronics, Xidian University, Xi'an 710071, China

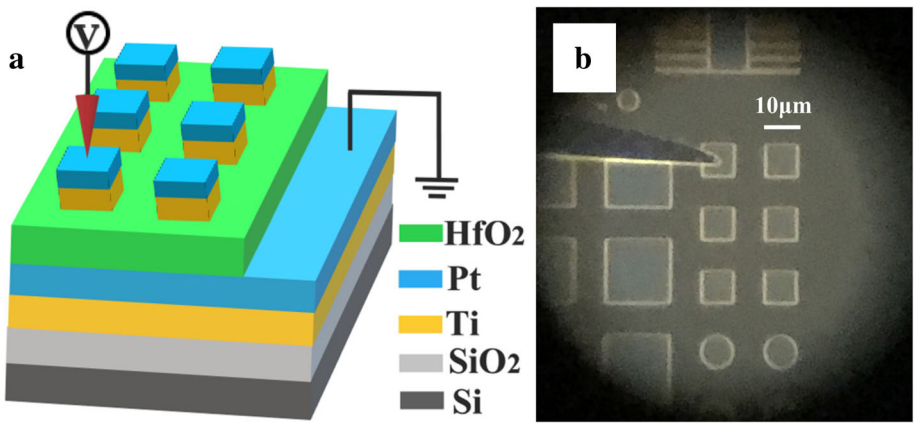

Fig. 1 The structure of the devices. **a** 3D model of the memristors. **b** Optical microscopy of the devices

devices, Al-doped devices show a distinct 74.1 eV peak of Al 2p in Fig. 2a, and the binding energy of Hf 4f has a certain increase in Fig. 2b. The ratio of Hf $4f_{5/2}$ to Hf $4f_{7/2}$ also increased for the doped devices. It is consistent with the other reports [14, 26, 27]. Al atoms bond to HfO2 structure to form Hf-Al-O, which results in the weaker and more easily broken Hf-O bonds.

For all the electrical measurements, the Ti TE was biased while the Pt BE was grounded. DC sweeps were performed by using a B1500A parameter analyzer (Santa Clara, CA, USA) with a source/measurement unit, and pulse electrical measurements with a waveform generator/fast measurement unit are also used. All the devices show high-resistance state (HRS) before a necessary electric forming process. Figure 3a shows the forming characteristic of the 10 μm × 10 μm Al-doped and non-doped devices. A current compliance during forming is necessary to protect the devices from being damaged. The initial resistance and forming voltage of non-doped device is larger. The oscillation in the low-voltage region of the non-doped device is because the current is lower than the measuring limit of the instrument. The reset process after the forming step is motivated by applying a negative voltage, as shown in Fig. 3a, and then the first set process is motivated. As the voltage amplitude of reset increases, the current of both two devices increase to a maximum larger than the limited current of forming and then decrease. The HRS currents of both two devices are several orders larger than that of the initial state at the same voltage. It suggests that there is still conductive filament that cannot be fused completely after reset. The typical set/reset I–V curves in Fig. 3b shows both typology of these two devices is bipolar operation mode [28]. The switching ratio and the set/reset voltage of Al-doped device are smaller than those of non-doped device, but its resistance state transformation process is more gentle, suitable as a multi-value storage device.

To clarify the switching mechanisms of the devices, the I–V curves are replotted in double logarithmic scale in Fig. 4. For both kinds of devices, the low-resistance

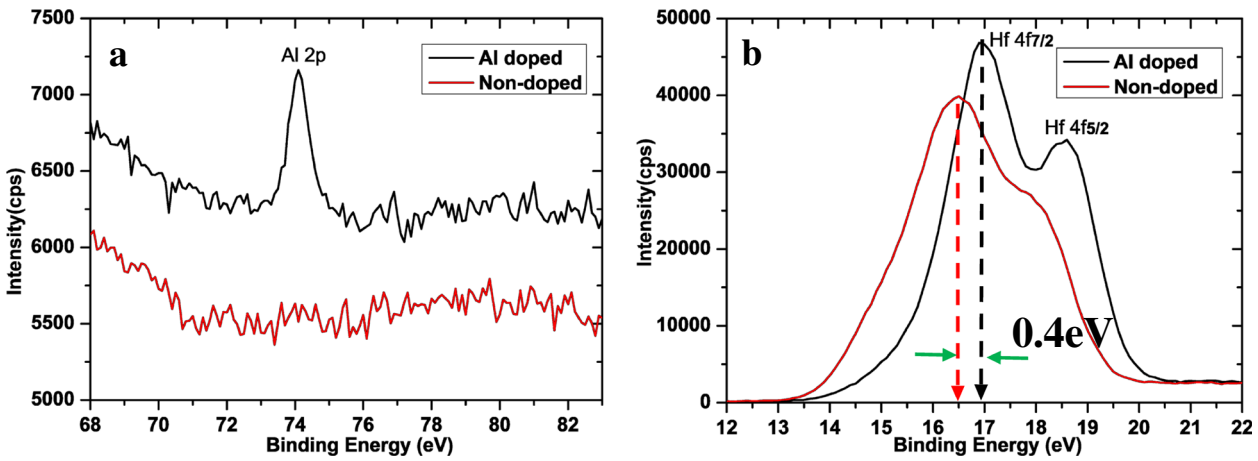

Fig. 2 The XPS of Al-doped and non-doped devices. **a** Al 2p and **b** Hf 4f are compared

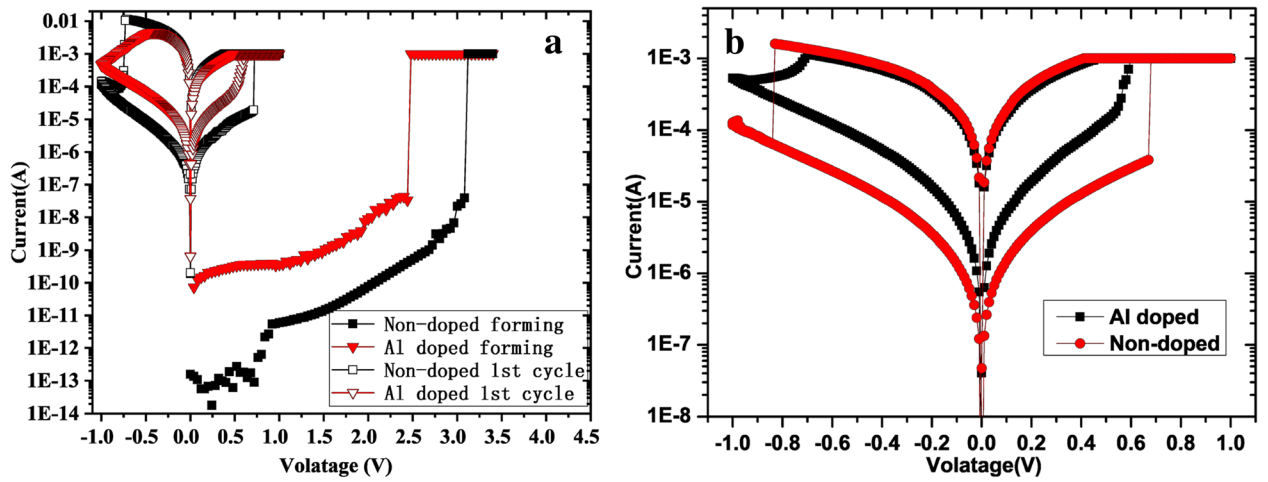

Fig. 3 The I/V characteristics of the devices. **a** The forming process and first cycle. **b** The typical set/reset process

curve exhibits a linear Ohmic behavior, which indicates the formation of conducting filaments in HfO_2 films during their setting [29, 30]. However, the high-resistance curves are quite different between these two kinds of devices. For the doped device, it is composed of three regions: the Ohmic region ($I \propto V$), the Child's law region ($I \propto V^2$), and the steep current increase region, which is accorded with the typical I–V characteristic of trap-controlled space charge limited current (SCLC) [31, 32]. The high-resistance curve of the non-doped device is composed of two regions: the Ohmic conduction ($I \propto V$) at the low-voltage region, and the linear fit of the $\ln I\text{-}V^{1/2}$ at high-voltage region (the inset of Fig. 4), confirming the Schottky emission mechanism [15, 33].

According to the features above, the microscopic mechanisms of the memristors are summarized as follows. For undoped devices, as the positive voltage applied to the titanium electrode increases, more and more oxygen ions generate in the HfO_2 and move toward the titanium electrode [34], producing titanium oxide [35]. At the same time, the oxygen vacancies accumulate at the interface between the platinum electrode and the HfO_2, forming conductive filaments gradually [36]. Therefore, current increases gradually with the voltage. The devices turn into low-resistance state (LRS) when the oxygen vacancies conducting filaments connect the TE and BE. While the titanium electrode applied with a negative voltage, the oxygen ions combine with the oxygen vacancies at the HfO_2/Pt interface [37], which leads to the lower oxygen

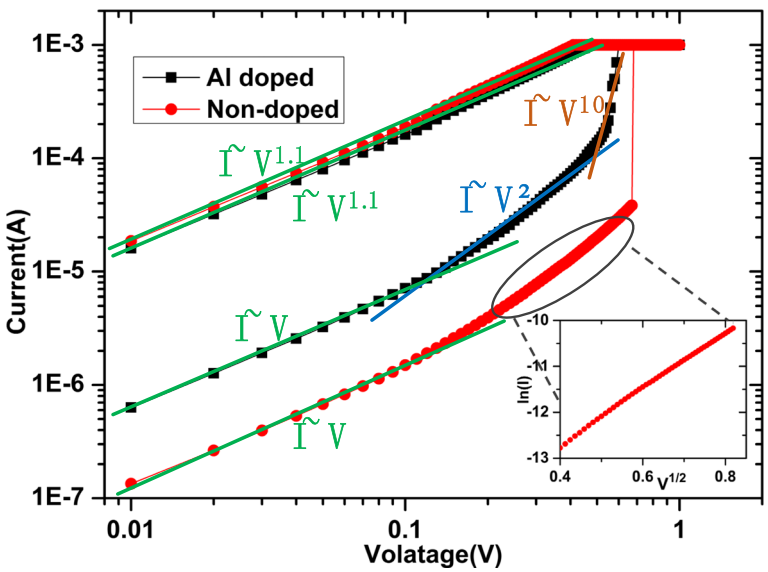

Fig. 4 The curve fitting of SET process in the double logarithmic coordinates

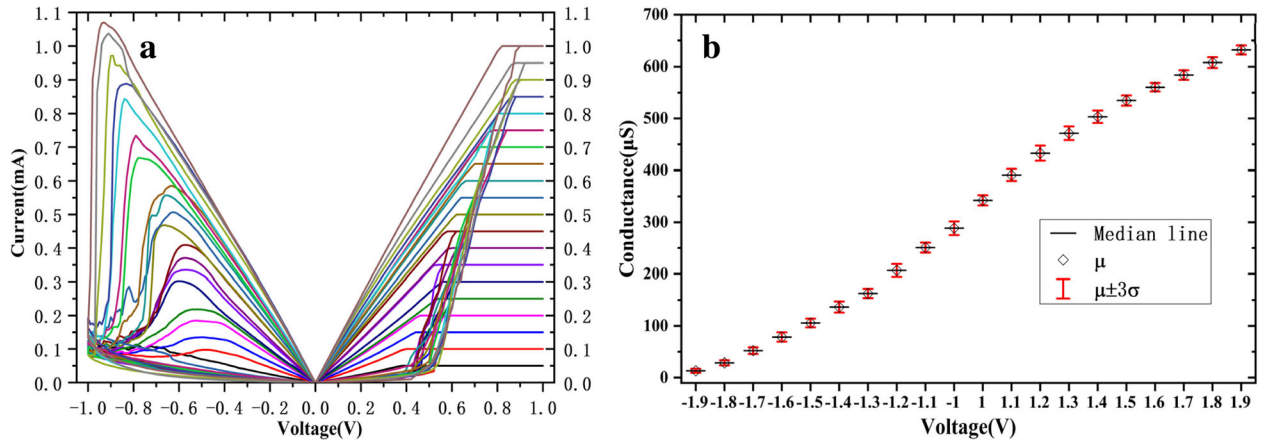

Fig. 5 The multi-value storage of the devices. **a** Transform resistance states by setting compliance currents. **b** 20 stable resistance states obtained by setting pulse voltage amplitude The pulse width and interval are both 500 μs

vacancy concentration and the higher Schottky barrier. When the reset voltage reached, the conductive filament is broken and the device is changed to HRS.

For Al-doped devices, Al atoms bond to HfO2 structure to form Hf-Al-O result in the weaker and more easily broken Hf–O bonds. The formation energy of oxygen vacancy is reduced. Therefore, the doping devices have a smaller resistance and a lower transition voltage. In undoped films, oxygen vacancies tend to accumulate along the grain boundaries [38, 39]. As a result, conductive filaments are few and thick. The resistance of the devices varies greatly with the conduction and breakage of the conductive filaments. In the doped films, oxygen vacancies are easily formed near the impurity atoms [35, 40, 41]. The uniform distribution of a large amount of impurities in the thin film makes the conductive filaments be formed by oxygen vacancies more controllable. Therefore, it is easier to achieve multiple resistance values.

The devices can be set to different steady resistance states by changing the current compliance of set process. Twenty stable resistance states are obtained by setting current compliance forming 0.5 mA to 10 mA with a step of 0.5 mA in Fig. 5a. As the resistance states set by DC sweep, the energy consumption is large, and the operation is complicated. On the other hand, the resistance values are easily locked in LRS when a large current compliance is used. This method is also unable to adjust the HRS. Twenty-level resistance states achieved by changing voltage amplitude of set and reset pulse. To avoid the possibility of current overshooting and set/reset failure, the voltage amplitude is limited between 1 V~1.9 V for SET and − 1 V~− 1.9 V for reset. It can be seen from the box diagram (Fig. 5b) that the allowed voltage range is divided into 20 values and the yield of the device is far exceeding the 3 σ level (99.73%). This is a common requirement in production. The disadvantage

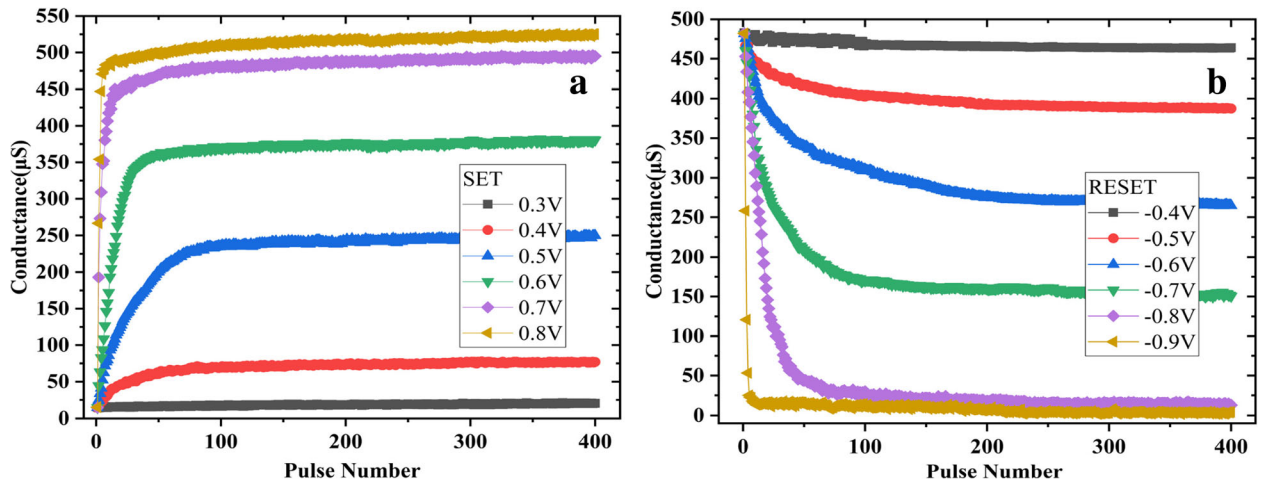

Fig. 6 The resistance adjusted by consecutive pulses. **a** Set process and **b** reset process

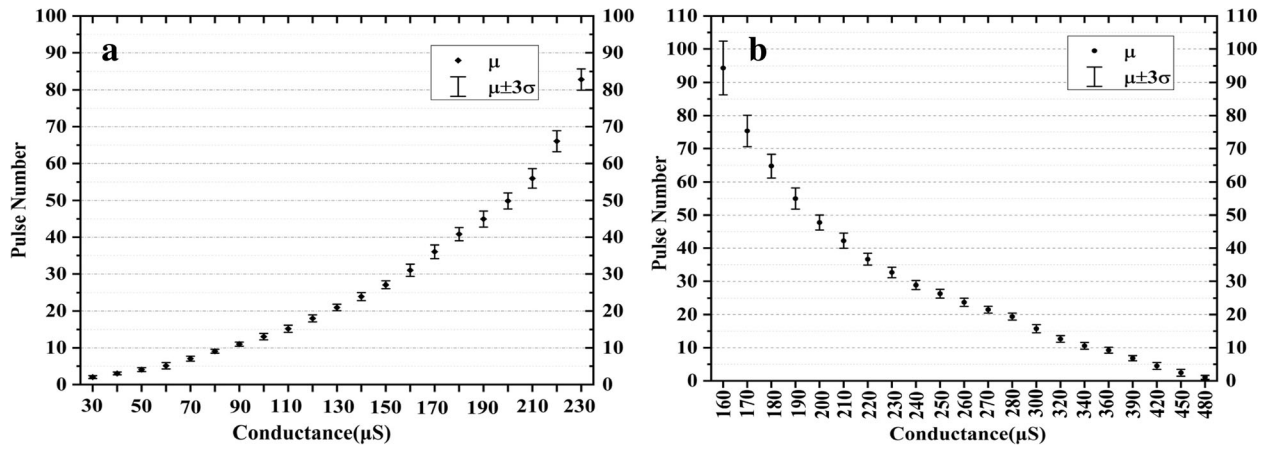

Fig. 7 Pulse number needed to set (**a**) or reset (**b**) the devices to 20 different levels

of this method is that the devices cannot be set directly from one HRS (LRS) to another HRS (LRS), but need to reset (set) to LRS (HRS) firstly, and then set to the target HRS (LRS). This increases the complexity and power consumption of the operation.

A better approach is shown in Fig. 6. The device conductance is incrementally increased or decreased by consecutive pulses. The pulse duration and interval are both 10 μs. The conductance is measured by a 0.1 V read pulse after each set/reset pulse. As seen in Fig. 6, the number of pulses needed in order to set/reset the devices to different levels depends on the voltage applied. The different resistant statues with 20 levels are obtained through set and reset by selecting 0.5 V as SET voltage and − 0.7 V as reset voltage respectively (Fig. 7). The device is reset to a HRS by 10 − 0.9V consecutive pulses every time before setting to the target status or set to a LRS by 10 0.8-V consecutive pulses before adjustment. Considering the same status present at both the set and reset process, there are 35 different statuses obtained totally. The deviation of pulse number needed for the two adjacent resistance states of set (reset) exceeds the 3 σ level. The disadvantage is that if the resistance values of the devices change greatly, the pulse number needed will be large and the operation speed will be slow.

To test the data retention of the devices, 20 devices are set/reset to a series of different resistance values, and keeping them on a heating table at 85 °C [42]. The resistance values were measured with a voltage of 0.1 V every 100 s. It can be seen from Fig. 8a that the resistance of the devices maintains stable after 10^4 s. In order to test the cycle reliability of the device, we repeated set and reset operation with a 1.8 V/500 μs set pulse and a − 1.8 V/500 μs reset pulse. After 10^3 cycles, the switching ratio of the device is still greater than 10 in Fig. 8b.

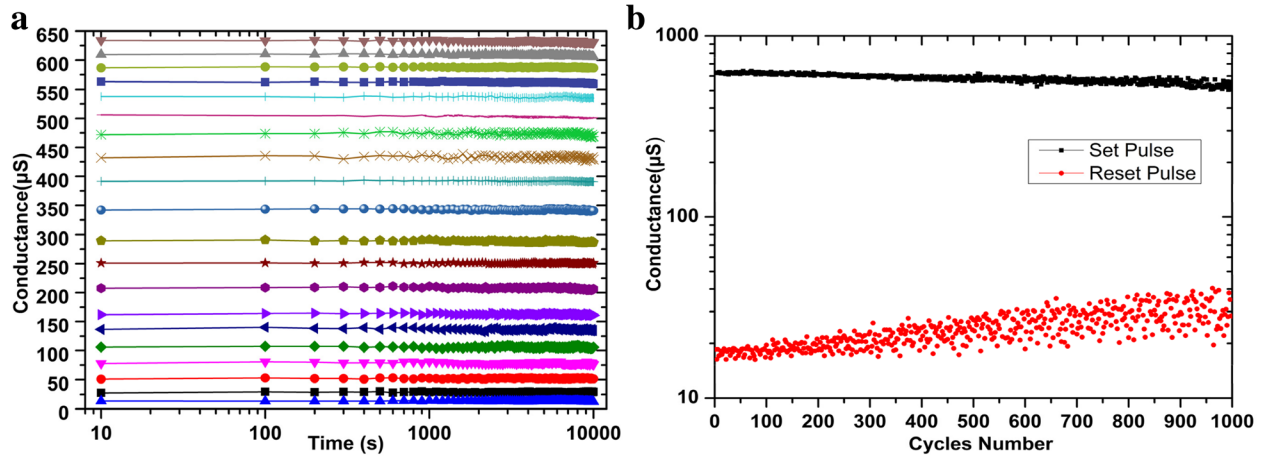

Fig. 8 The reliability tests of the devices. **a** Data retention characteristics after set/reset pulse operations. **b** Cycles endurance curves for set/reset pulse operations

Conclusions

The proposed Al-doped HfO_2 memristor shows a gradual and stable set/reset performance. By fitting the curve of set process of Al-doped and undoped devices, it is found that, in HRS, the undoped device follow Schottky emission mechanism, while the Al-doped device follow SCLC conductive mechanism. The microscopic physical mechanism of resistance change is also discussed. In addition, the multi-value storage of the device was confirmed by changing the compliance current, adjusting the set/reset pulse voltage amplitude and using the consecutive short pulses. Finally, we tested the reliability of the devices to prove that it has a data retention of more than 10^4 s (85 °C) and a switching ratio greater than 10 after 10^3 cycles.

Abbreviations

ALD: Atomic layer deposition; BE: Bottom electrode; CMOS: Complementary metal oxide silicon; HfD-04: $MeCp_2HfMe(OMe)Hf$; HRS: High-resistance state; LRS: Low-resistance state; NVM: Non-volatile memory; SCLC: Space-charge-limited current; TE: Top electrode; TMA: Trimethylaluminum; XPS: X-ray photoelectron spectroscopy

Acknowledgements

The authors gratefully acknowledge the support provided by the Fundamental Research Funds for the Central Universities and the Innovation Fund of Xidian University.11 project (grant no. B12026)

Authors' Contributions

LW generated the research idea, analyzed the data, and wrote the paper. JbL and SlW carried out the experiments and measurements. HxL and XW have given final approval of the version to be published. All authors read and approved the final manuscript.

Funding

The authors gratefully acknowledge the financial support for this work from the National Natural Science Foundation of China (grant no. U1866212), the Foundation for Fundamental Research of China (grant no. JSZL2016110B003), the major Fundamental Research Program of Shaanxi (grant no. 2017ZDJC-26), and the China Postdoctoral Science Foundation (grant no. 2018M633460).

Availability of Data and Materials

All data generated or analyzed during this study are included in this published article.

Competing Interests

The authors declare that they have no competing interests.

Received: 31 December 2018 Accepted: 15 May 2019
Published online: 28 May 2019

References

1. Hickmott TW (1962) Low-frequency negative resistance in thin anodic oxide films. J Appl Phys 33:2669–2682
2. Chua L (1971) Memristor-The missing circuit element. IEEE Trans Circuit Theory 18:507–519
3. Strukov DB, Snider GS, Stewart DR et al (2008) The missing memristor found. Nature 453:80–83
4. Asamitsu A, Tomioka Y, Kuwahara H et al (1997) Current switching of resistive states in magnetoresistive manganites. Nature 388:50–52
5. Watanabe Y, Bednorz JG, Bietsch A et al (2001) Current-driven insulator–conductor transition and nonvolatile memory in chromium-doped $SrTiO_3$ single crystals. Appl Phys Lett 78:3738–3740
6. Xu N, Liu L, Sun X et al (2008) Characteristics and mechanism of conduction/set process in TiN/ZnO/Pt resistance switching random-access memories. Appl Phys Lett 92:587
7. Rohde C, Choi BJ, Jeong DS et al (2005) Identification of a determining parameter for resistive switching of TiO_2 thin films. Appl Phys Lett 86:262907
8. Wedig A, Luebben M, Cho DY et al (2016) Nanoscale cation motion in TaOx, HfOx and TiOx memristive systems. Nat Nanotechnol 11:67
9. Sangwan VK, Lee HS, Bergeron H et al (2018) Multi-terminal memtransistors from polycrystalline monolayer molybdenum disulfide. Nature 554:500–504
10. Liu B, Zhiwei L, In-Shiang C et al (2018) Programmable synaptic metaplasticity and below femtojoule spiking energy realized in graphene-based neuromorphic memristor. ACS Appl Mater Interfaces 10:20237–20243
11. Frank MM, Wilk GD, Starodub D et al (2005) HfO_2 and Al_2O_3 gate dielectrics on GaAs grown by atomic layer deposition. Appl Phys Lett 86:87–14
12. GUSEV EP et al (2001) Ultrathin high-K gate stacks for advanced CMOS devices. IEDM 2001. IEEE 2001: 20.1. 1-20.1. 4.
13. Yu S, Gao B, Dai H et al (2010) Improved uniformity of resistive switching behaviors in HfO_2 thin films with embedded Al layers. Electrochem Solid St 13:H36–H38
14. Lin YS, Zeng F, Tang SG et al (2013) Resistive switching mechanisms relating to oxygen vacancies migration in both interfaces in Ti/HfO_x/Pt memory devices. J Appl Phys 113:064510
15. Lu C, Yu J, Chi XW et al (2016) Self-compliance Pt/HfO_2/Ti/Si one-diode-one-resistor resistive random access memory device and its low temperature characteristics. Applied Physics Express 9:041501
16. Wang Y, Liu Q, Long S et al (2010) Investigation of resistive switching in Cu-doped HfO_2 thin film for multilevel non-volatile memory applications. Nanotechnology 21:045202
17. Yang YC, Pan F, Liu Q et al (2009) Fully room-temperature-fabricated nonvolatile resistive memory for ultrafast and high-density memory application. Nano Lett 9:1636–1643
18. Lee HY, Chen PS, Wu TY et al (2008) Low power and high speed bipolar switching with a thin reactive Ti buffer layer in robust HfO_2 based RRAM. IEDM 2008. IEEE 2008:1–4
19. Zhou YX, Li Y, Su YT et al (2017) Nonvolatile reconfigurable sequential logic in a HfO_2 resistive random access memory array. Nanoscale 9:6649–6657
20. Jo SH, Chang T, Ebong I et al (2010) Nanoscale Memristor Device as Synapse in Neuromorphic Systems. Nano Lett 10:1297–1301
21. Li Y, Zhong Y, Zhang J et al (2014) Activity-dependent synaptic plasticity of a chalcogenide electronic synapse for neuromorphic systems. Sci Rep 4:4906
22. Yang X, Fang Y, Yu Z et al (2016) Nonassociative learning implementation by a single memristor-based multi-terminal synaptic device. Nanoscale 8:18897
23. Yang JJ, Strukov DB, Stewart DR (2013) Memristive devices for computing. Nat Nanotechnol 8:13–24
24. Gao B, Chen B, Zhang F et al (2013) A novel defect-engineering-based implementation for high-performance multilevel data storage in resistive switching memory. IEEE Trans Electron Devices 60:1379–1383
25. Cianci E, Molle A, Lamperti A et al (2014) Phase stabilization of Al:HfO_2 grown on $In_xGa_{1-x}As$ substrates (x=0, 0.15, 0.53) via trimethylaluminum-based atomic layer deposition. ACS Appl Mater Interfaces 6:3455–3461
26. Park PK, Cha ES, Kang SW (2007) Interface effect on dielectric constant of HfO_2/Al_2O_3 nanolaminate films deposited by plasma-enhanced atomic layer deposition. Appl Phys Lett 90:232906
27. Chiou YK, Chang CH, Wang CC et al (2007) Effect of Al incorporation in the thermal stability of atomic-layer-deposited HfO_2 for gate dielectric applications. J Electrochem Soc 154:G99–G102
28. Waser R, Aono M (2007) Nanoionics-based resistive switching memories. Nat Mater 6:833–840
29. Celano U, Chen YY, Wouters DJ et al (2013) Filament observation in metal-oxide resistive switching devices. Appl Phys Lett 102:121602
30. Chen JY, Hsin CL, Huang CW et al (2013) Dynamic evolution of conducting nanofilament in resistive switching memories. Nano Lett 13:3671–3677
31. Lampert MA, Mark P (1970) Current injection in solids. Academic Presslnc, New York
32. Kinoshita K, Tamura T, Aoki M et al (2006) Bias polarity dependent data retention of resistive random access memory consisting of binary transition metal oxide. Appl Phys Lett 89:103509
33. Sze SM (1981) Physics of semiconductor devices, 2nd edn. John Wiley and Sons, New York
34. Sowinska M et al (2012) Hard x-ray photoelectron spectroscopy study of the electroforming in Ti/HfO2 -based resistive switching structures. Appl Phys Lett 100:233509

35. Ma G, Tang X, Su H et al (2014) Effects of standard free energy on NiO bipolar resistive switching devices. IEEE Trans Electron Devices 61:1237–1240
36. Gu CJ, Ang DS et al (2016) Understanding the switching oxide defect formation and recovery on HfOx based RRAM device. ECS J Solid State Sci Technol 5:N90–N95
37. Goux L, Wang XP, Chen YY et al (2011) Roles and effects of TiN and Pt electrodes in resistive-switching HfO2 systems. Electrochem Solid St 14: H244–H246
38. Bersuker G, Gilmer DC, Veksler D et al (2011) Metal oxide resistive memory switching mechanism based on conductive filament properties. J Appl Phys 110:2632–2636
39. Vandelli L, Padovani A, Larcher L et al (2011) Comprehensive physical modeling of forming and switching operations in HfO_2 RRAM devices. IEDM IEEE 2011:17.5.1–17.5.4
40. Clima S, Govoreanu B, Jurczak M et al (2014) HfO_x as RRAM material—first principles insights on the working principles. Microelectron Eng 120:13–18
41. Traore B, Blaise P, Vianello E et al (2014) Microscopic understanding of the low resistance state retention in HfO2 and HfAlO based RRAM. IEDM IEEE 2014: 21.5. 1-21.5.4
42. Yang PK, Ho CH, Lien DH et al (2015) A fully transparent resistive memory for harsh environments. Sci Rep 5:15087

Publisher's Note